NATO Advanced Study Institute, "The Study of Fast Processes and Labile Species in Chemistry and Molecular Biology Using Ionizing Radiation", Capri, Italy, September 7-18, 1981

Conf-8109205--1

DISCLAIMER

CONF-8109205--1

DE83 007707

STRUCTURE AND DYNAMICS OF PARAMAGNETIC TRANSIENTS BY PULSED EPR AND NMR DETECTION OF NUCLEAR RESONANCE

Alexander D. Trifunac

Chemistry Division
Argonne National Laboratory
Argonne, Illinois 60439
U.S.A.

ABSTRACT

Structure and dynamics of transient radicals in pulse radiolysis can be studied by time resolved EPR and NMR techniques. EPR study of kinetics and relaxation is illustrated. The NMR detection of nuclear resonance in transient radicals is a new method which allows the study of hyperfine coupling, population dynamics, radical kinetics, and reaction mechanism.

INTRODUCTION

The study of transient radicals produced by pulsed radiolysis, as carried out using magnetic resonance tools, involves the determination of radical hyperfine coupling constants, kinetics, and spin population dynamics. The coupling constants not only provide a definite spectral assignment but also provide insight into spin delocalization on the radical and thus its structure. The determination of radical kinetics is experimentally useful when radicals without distinct optical absorption bands are investigated. In addition, the magnetic resonance methods allow us to study various manifestations of the spin system, i.e., non-equilibrium population dynamics, that is, CIDEP and CIDNP, and spin relaxation phenomena. The study of Chemically Induced Magnetic Polarization (CIMP) provides useful insights into radical reaction mechanisms.

MASTER

TIME RESOLVED EPR

The hyperfine coupling, i.e., the electron spin density at various nuclei, tells us about the structure of the radical species. The majority of EPR studies deal with the observation and analysis of hyperfine couplings of a great variety of radicals.

Time resolved EPR suffers from a decrease of sensitivity, and from line broadening at the very short times (<1 μsec) so one often cannot resolve the very closely spaced lines. Depending on the experimental conditions, hyperfine couplings that are smaller than 1-2 gauss cannot be resolved. One can still analyze the width of the whole spectrum and get an idea of the size of the hyperfine coupling, but there are better methods for that. Time resolved EPR is best suited for the study of transient radicals that have well resolved lines.

I want to emphasize again that all this refers to the study of very short-lived radicals (μsec lifetimes). When radicals live hundreds of μsec, one can do conventional high resolution EPR.

In my view, most of the usefulness of time-resolved EPR studies has been in the area of dynamics, or in observing transient radicals not seen otherwise. The structural studies of various radical hyperfine couplings, while important, have been secondary.

Kinetics and Relaxation

Both kinetic and relaxation data are obtainable by studying the time dependence of transient (z) magnetization (1,2).

The transient magnetization develops and decays in time. In the reactions where a single radical is present, e.g., $\cdot CH_2COO^-$, the creation and destruction of magnetization is describable in terms of a kinetic equation (1):

$$\dot{M}_z = -T_R(t)^{-1} M_z - T_1^{-1}(M_z - M_z^0) + \dot{E}(t) M_z^0 \qquad (1)$$

The loss in magnetization M_z occurs because of the chemical decay of radicals where the lifetime $T_R(t)$ is defined as:

$$T_R(t)^{-1} = \left(\frac{\dot{R}}{R}\right) = -\left(\frac{d \ln R}{dt}\right) \qquad (2)$$

where R is the concentration of radicals.

This definition of $T_R(t)$ is general enough as it allows the quantity to be either positive or negative (radical creation or

decay). The second term in eq. (1) describes spin relaxation of M_z toward its equilibrium value $M_z^0(t)$ with time constant T_1. M_z^0 is proportional to the radical concentration at time (t) so from eq. (2):

$$\dot{M}_z^0 = T_R(t)^{-1} M_z^0 \tag{3}$$

The last term in eq. (1) represents the creation of the non-equilibrium population by chemical reaction. This is expressed through a time dependent enhancement factor E(t). When we have, as in the acetate radical, a dominant bimolecular decay, we define a second order lifetime T_c where k_d is the bimolecular rate constant:

$$T_c^{-1} = 2k_d R(0) \tag{4}$$

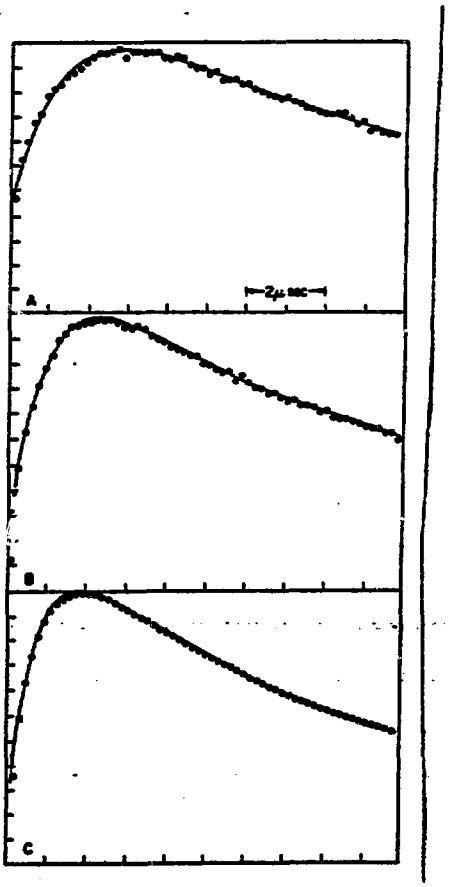

Figure 1. High field line of $\cdot CH_2CO_2^-$ radical at three radical concentrations. Data (circles) and computer fit (solid line) are illustrated.

The equations illustrated above can be numerically integrated by computer and used to analyze the experimental data. M_Z is computed for various values of T, T_C, and E. Additional baseline offsets, first order rate constants, and initial enhancement can be considered as well. An example of such curve fitting is illustrated in Figure 1. By doing such data analysis, one can determine T_C, i.e., the second order reaction rate, or by using a radical with known kinetics, one can determine its reactions with another substrate by determining the psuedo first order rate constants.

This analysis using pulsed EPR represents a considerable simplification over the type of analysis used for CW-EPR. Still, it is not as straightforward as analysis of optical data. The polarization and relaxation are the complicating factors. However, the study of these complicating factors provides additional insights into the radical reaction dynamics. For example, if we examine how radical relaxation varies (actually decreases) as radical concentration increases (as we increase the dose) we can learn about the details of radical collisions (3). Figure 2 illustrates the results. The various ways of determining T_1 all tell us that there is a remarkable speeding up of spin relaxation at high radical concentrations. The explanation for this is that spin-spin interaction (Heisenberg exchange) becomes more prevalent at high radical concentrations. This exchange interaction is

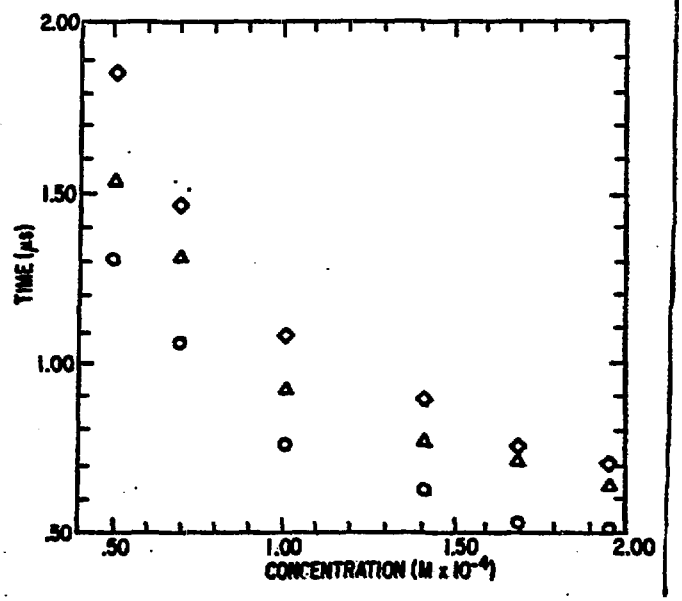

Figure 2. T_1 measurements at various $\cdot CH_2CO_2^-$ radical concentrations: ○- asymptotic analysis; △- inversion recovery; ◇- least squares computer fitting.

important during radical encounters only, and thus we have a measure of the non-reactive encounters by measuring the decrease of T_1 with radical concentration. On the other hand, the measurement of radical kinetics gives information on the reactive encounters. From this we conclude that there are 2 to 5 times more non-reactive than reactive encounters. Of course, the analysis is considerably more complex than I have indicated, and there are several complicating factors. The problems arise at extremely high radical concentration where substantial second order decay occurs during the time (τ) between the microwave pulses. This causes the observed signal (M_z) to appear smaller than it actually is. At lower radical concentrations, or if the radical decay is first order, the problem does not arise.

In closing, pulsed EPR is the method that has superior time resolution, comparable sensitivity, and simplified kinetic analysis compared to the continuous wave time-resolved EPR. The problems of spectral resolution at very short times are similar in the two approaches, and there are problems peculiar to the pulsed EPR method. But, as I will illustrate later, inherent advantages of the pulsed EPR approach make this, in the opinion of the author, a method of choice. Remember that the pulsed EPR spectrometer components are just added to the CW EPR bridge, so without much difficulty, one can do either.

NMR DETECTION OF NUCLEAR RESONANCE

The previously illustrated NMR experiment is a steady-state experiment. A straightforward modification of the experiment opens a way to a new spectroscopic method (4).

When a radio frequency (rf) irradiation is supplied to the reacting sample after irradiation with the electron beam pulse, the nuclear spin populations in the diamagnetic products show substantial perturbations (Figure 3). The frequency applied during the radical lifetime is the ENDOR frequency (5-50 MHz) perturbing the electron nuclear spin population in the transient radical. Our experiment, as applied in pulse radiolysis, is based on a flow system utilizing two magnets. The ability to use a variable magnetic field for irradiation and the pulsed rf irradiation makes our experiment a time resolved one and opens a wide range of possibilities. The technique of NMR-detected nuclear resonance (NMR-NR) provides information about the mechanism and kinetics of radical reactions and about populations of the magnetic energy levels of transient radicals in all magnetic fields, and is a very accurate method for determining hyperfine coupling constants of transient radicals.

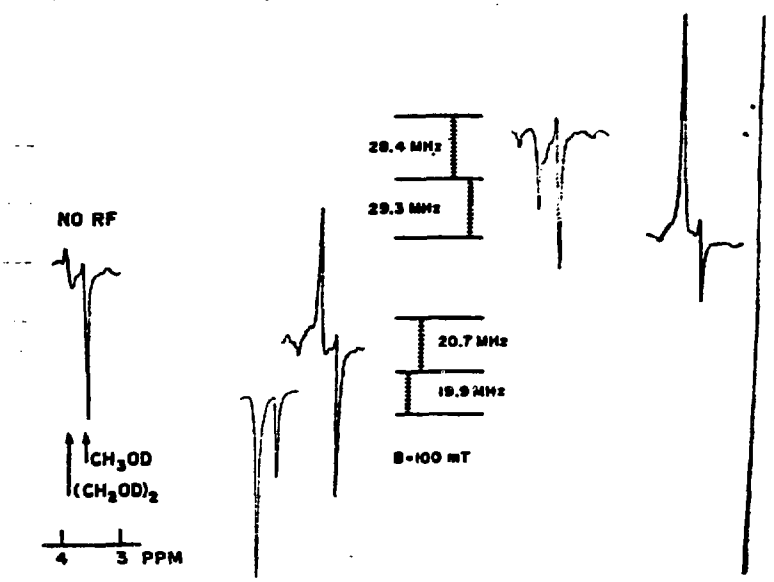

Figure 3. The NMR-NR effect in pulse radiolysis of 0.1 M. Methanol in D_2O at 100 mT (1000 gauss). (A) NMR spectrum observed when electron irradiation is carried out with appropriate rf frequency (spectra on the right) and without rf (spectrum on the left).

For the purpose of illustration, we consider the methanol radiolysis. Pulse radiolysis of aqueous (D_2O) methanol initially produces the radicals ·OD, D·, and e^-_{aq} as well as other species. The dominant reaction and polarization pathways in the subsequent methanol reactions are listed below in Eqs. 5-8.

$$CH_3OD \xrightarrow{\cdot OD} \cdot CH_2OD \qquad (5)$$

$$2(\cdot CH_2OD) \longrightarrow (CH_2OD)_2 \qquad (6)$$

$$\cdot CH_2OD + D\cdot \longrightarrow CH_2DOD \qquad (7)$$

$$e^-_{aq} + \cdot CH_2OD \longrightarrow CH_2OD^- \xrightarrow{D^+} CH_2DOD \qquad (8)$$

The NMR-NR effect considered herein is shown in Figure 3. The intensity of the NMR signal due to ethylene glycol is plotted as a function of the frequency of the rf irradiation pulse supplied during the lifetime of the $\cdot CH_2OD$ radical to the electron

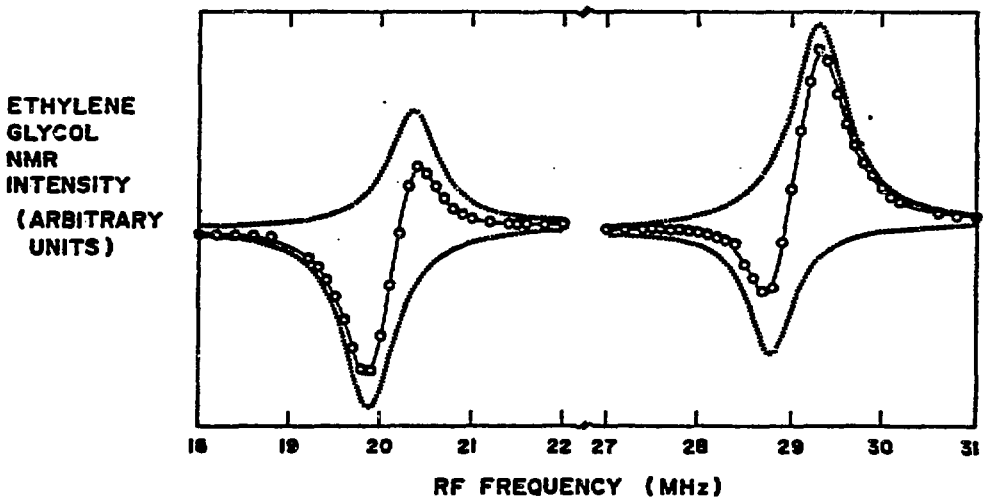

Figure 4. NMR-NR effect as in Figure 3. The experimental points (circles) were fitted with Lorentzian components (dotted curves) of the solid curve.

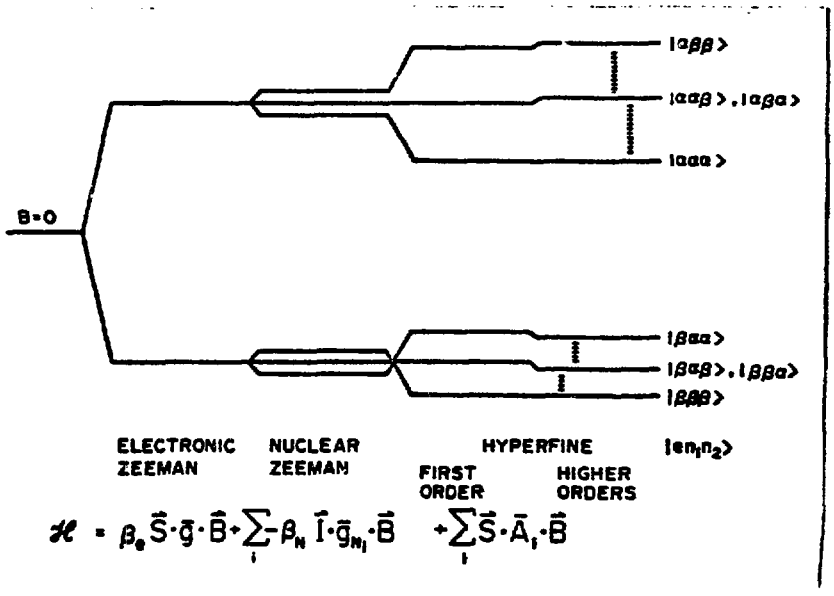

Figure 5. Energy levels and the spin Hamiltonian for spin systems like $\cdot CH_2OH$ radical in intermediate magnetic fields (~100 mT).

irradiation cell, which is in a 100 mT (1000 gauss) magnetic field (Figure 4).

The four peaks in the observed curve correspond to the four nuclear transitions of the methanol radical, $\cdot CH_2OD$, as shown in Figure 4. Transition frequencies were calculated using Breit-Rabi type formulas (5), where the g-factor and isotropic hyperfine parameter used were g = 2.00317 and a = -1.750 mT, respectively (6). Clearly, at the magnetic field used, the energy levels do not have a first order pattern (Figure 5). Small effects due to hydroxyl deuterium and interaction between the two equivalent protons can be ignored. Obviously, we can determine hyperfine coupling constants with great accuracy. The accuracy is comparable to the ENDOR method, but so far ENDOR experiments on transient radicals have not been achieved.

Another rather straightforward application of NMR-NR is in providing a connection between the radicals and their fragments incorporated into reaction products. The radical system in the radiolysis of methanol-methyl iodide mixture in D_2O is used to illustrate this point (Eqs. 9-13, Figure 6),

$$CH_3 \xrightarrow{e^-_{aq}} \cdot CH_3 \qquad (9)$$

$$CH_3OD \xrightarrow{\cdot OD} \cdot CH_2OD \qquad (10)$$

$$\cdot CH_2OD + \cdot CH_3 \longrightarrow CH_3CH_2OD \qquad (11)$$

$$2(\cdot CH_3) \longrightarrow CH_3CH_3 \qquad (12)$$

$$\cdot CH_3 + \cdot D \longrightarrow CH_3D \qquad (13)$$

and the reactions of the $\cdot CH_2OD$ radical, as in methanol radiolysis (Eqs. 5-8).

Figure 6A shows the CIDNP spectrum obtained during the pulse radiolysis of an equimolar mixture of methanol and methyl iodide. The polarized products observed are methane (0.6 ppm), the methyl group of ethanol (1.6 ppm), methyl iodide (2.5 ppm), and the methylene group of ethanol (4.0 ppm). The weak emission at 3.1 ppm was not identified. When rf at 19.900 MHz is applied (Figure 6B), only the products from the $\cdot CH_2OD$ fragment are affected. These signals are observed at 4.0 ppm, which illustrate the strong effect on the quartet from ethanol (ethylene glycol would also be within this intense signal), and at 3.6 ppm, which shows an emission for CH_2DOD not observed in Figure 6A. For a determination of which polarizations arise from the $\cdot CH_3$ radical, a radio frequency of 36.500 MHz is applied. The results which are shown in Figure 6C indicate the signals affected are methane at 0.6 ppm, which

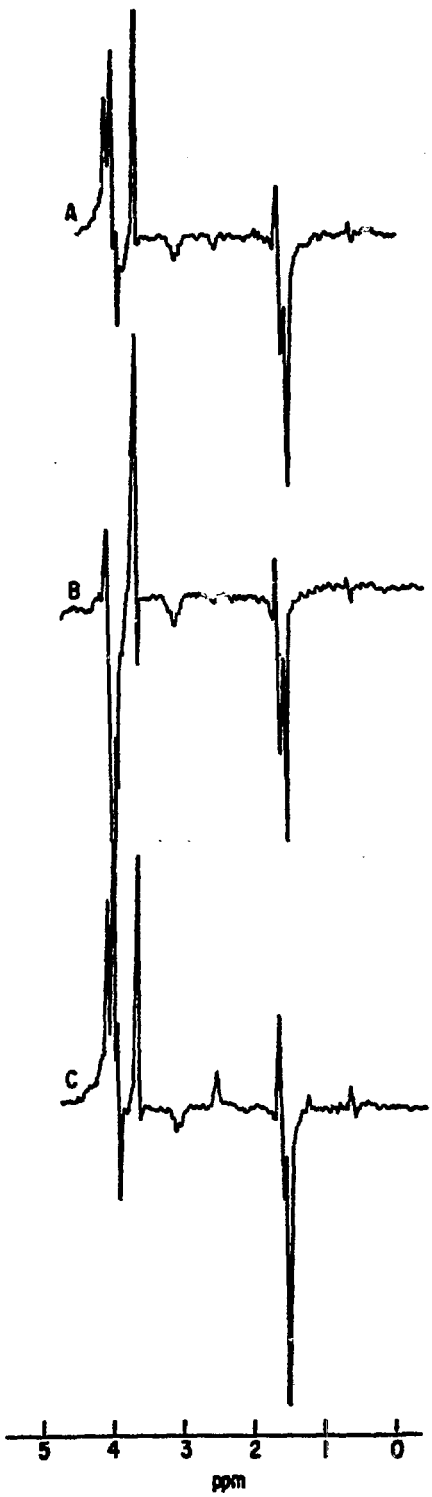

Figure 6. Pulse radiolysis in methanol-methyl iodide in D_2O at 100 mT: (A) with electron beam; (B) A with rf at 19.9 MHz; (C) A with rf at 36.5 MHz.

exhibits a slight increase in intensity, methyl iodide at 2.5 ppm, which shows complete inversion of its signal as compared to Figure 6A, and the triplet of methanol at 1.6 ppm, showing substantial increase in intensity. Interestingly, ethane is even observed at 1.2 ppm (weak enhanced absorption) which would have gone undetected in Figure 6A. In a more complex radical reaction system, where it may be less obvious what part of the radical product comes from which radical, the NMR-NR approach should provide a beneficial adjunct to the CIDNP study.

In the course of our study, it became apparent that lower rf power was needed to effect slower reacting (longer lived) radicals. For example, in the methanol radiolysis glycol polarization can be influenced at very low rf power while even at the highest rf power available, the effect on methanol is always smaller. Thus, different radical lifetimes of the CIDNP cage product (methanol) vs. escape product (glycol) are differentiated.

Short rf pulses (0.5-2 μ-sec) are used to probe the time dependence of the NMR-NR signal intensity. The plots thus obtained are shown in Figure 7. The signal intensity vs. time

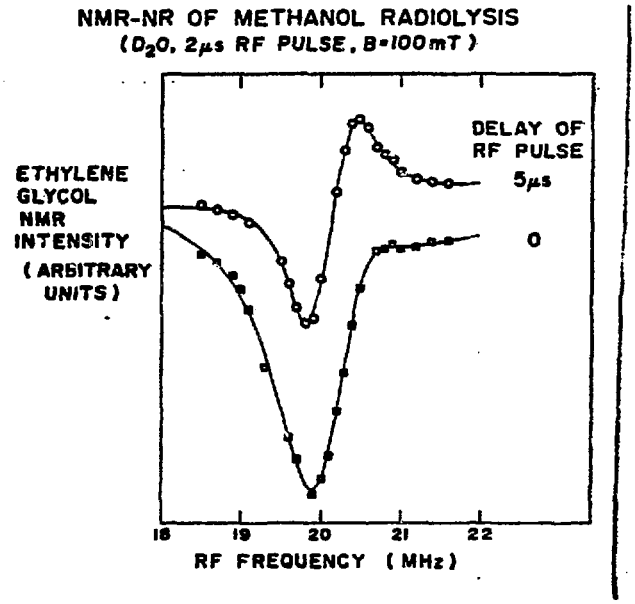

Figure 7. Time dependence of NMR-NR effect in methanol radiolysis.

of the rf pulse after the electron beam (at time zero) should represent radical kinetics as long as the nuclear T_1 in the radicals is appreciably longer than the chemical decay (second-order half-life) of the radicals. This is the case with the $\cdot CH_2OD$ radical in the concentration range utilized (10^{-3}–10^{-4} M radical concentration/pulse).

From the second-order plot, the second-order half-life of the $\cdot CH_2OH$ radicals is ~6 μs. The radical concentration is evaluated to be 6×10^{-4} M since the bimolecular rate constant for $\cdot CH_2OH$ is known $(3 \pm 1) \times 10^8$ M^{-1} s^{-1}) (10). One can also obtain the radical concentration directly from the absorbed electron beam intensity. This latter approach yields a radical concentration of 10^{-3} M and a second-order rate constant of 1.6×10^8 M^{-1} s^{-1}. However, given the variables involved in the determination of the radical concentration, it is preferable to calibrate the experimental system by using a radical with a known second-order rate constant, as we have illustrated above. The accuracy of rate constants obtained by NMR-NR should compare quite favorably to those obtained by usual optical or fast EPR methods.

The kinetic applications of NMR-NR have yet to be fully understood and developed as we have to analyze fully the dynamic problems encountered.

CIDNP and CIDEP Contributions

We present a model for the observed intensities based on the radical pair theory of CIDEP and CIDNP (7). Again, we consider the NMR-NR spectrum of $\cdot CH_2OD$ radical in methanol radiolysis, observed through ethylene glycol product. The Boltzman distribution is overshadowed by these polarizations, as determined by the presence of only a barely detectable ethylene glycol NMR signal in the irradiation solution after the nuclear spins have had time to relax. Populations will be predicted for the $\cdot CH_2OD$ energy levels using the radical pair theory of CIMP (8), for various possible pairs involving $\cdot CH_2OD$. An adequate spin Hamiltonian for a radical pair is

$$\mathcal{H} = \beta H\cdot(g_1 S_1 + g_2 S_2) - J(1/2 + 2S_1\cdot S_2) + \sum_i a_{1i} S_1\cdot I_i + \sum_k a_{2k} S_2\cdot I_k \qquad (14)$$

where the first term represents the electronic Zeeman energy for the two unpaired electrons. S_1 and S_2 are the electronic spin operators for the two components. The next term represents the scalar exchange interaction of magnitude 2J and the remaining two terms represent the isotropic components of the hyperfine interactions in the two members of the pair. The nuclear Zeeman interaction, although significant in the calculation of energies, is not required for calculating polarizations. In each case considered, two freely diffusing radicals form the pair (i.e., so-called F-pair). During the initial encounter, those pairs with singlet electronic spin phasing tend to form product (with no CIMP), leaving behind predominantly triplet radical pairs. Combination products, in which the members of the pair react during a subsequent encounter, will be favored by a rapid singlet-triplet crossing rate, whereas scavenging products, with reaction between a member of the radical pair and a freely diffusing radical, will be favored by slow singlet-triplet crossing. Nuclear spin polarization (CIDNP) results from this selection process. Electron spin polarization (CIDEP) also develops after there is an excess of triplet radical pair character, through intersystem crossing and exchange during radical encounters. The singlet-triplet crossing rate is given by

$$a_n = (2h)^{-1}[(g_1 - g_2)\beta H + \sum_i a_{1i} m_{1i} - \sum_j a_{2j} m_{2j}] \qquad (15)$$

where g_1 is the g-factor for radical 1 and a_{1i} and m_{1i} are the hyperfine constant and nuclear spin quantum number, respectively, for nucleus k of radical 1. The relationship in Eq. 15 applies to the high applied magnetic field case, in which non-secular

terms in the electron spin can be ignored and only S-T_0 mixing (not S-$T_{\pm 1}$) is considered.

Since we can do experiments using various magnetic fields, we have chosen for this illustration H = 100 mT, because the four nuclear transitions of $\cdot CH_2OD$ are then easily resolvable (Figure 5). At higher fields, the transition frequencies approach a first order pattern, reducing the observed effect due to overlap of positive and negative peaks. The signal-to-noise ratio also deteriorates because the NMR-NR effect is smaller, relative to the increased CIDNP net effect which arises principally from the e^-_{aq} + $\cdot CH_2OD$ pair which has a large g-value difference. At lower applied fields, however, deviations from the high field approximation may become significant and the intense H_1 (rf) fields cannot be used if one wishes to observe well resolved NMR-NR transitions. Of course, the larger the nuclear hyperfine coupling, the higher is the magnetic field one can utilize.

It will be useful to consider separately the possible contributions of the net and multiplet effects, which arise from the first term and the last two terms, respectively, of the right-hand side of Eq. 15. In usual CIMP spectra, the net effect gives rise to an equal polarization for each of the lines in an EPR or NMR multiplet, whereas the multiplet effect has zero as the sum of the polarizations in each multiplet. Irradiating $\cdot CH_2OD$ with rf will affect these spin level populations. A 13 μs rf pulse beginning 0.5 μs before the electron beam pulse was used. With the maximum available H_1 in the 10-20 mT range, a $\pi/2$ pulse would be 2-4 μs. However, the reactive transient radicals have a distribution of lifetimes, creating a range of effective pulse widths (tip angles). It is not feasible at this time to treat quantitatively the effects on the populations caused by a range of rf pulse tip angles. Thus, we will qualitatively consider the rf-induced population shifts by assuming saturation (i.e., equalization of populations), even though saturation may not be occurring. This assumption leads to predicted relative NMR-NR intensities which agree with the experimental spectrum when the ratio of the population shifts due to the nuclear and electronic multiplet effects (n_M/e_M) is 1.7. The value of n_N/e_M, the ratio between the magnitudes of the nuclear net and electronic multiplet effects obtained from the observed peak areas, is small relative to the estimated uncertainties in the areas. NMR-NR spectra measured as a function of time using 2 μs rf pulses (Figure 7) are qualitatively similar to Figure 4, but vary in the ratio n_M/e_M. Not surprisingly, this ratio is also different for other chemical systems. Even though the present data are integrated over a range of radical lifetimes during which CIMP develops and relaxes and radical decay takes place, it has been possible, using NMR-NR, to obtain information about relative energy level populations in $\cdot CH_2OD$ that is not available from CIDEP alone or otherwise. As predicted for high fields, the CIDEP

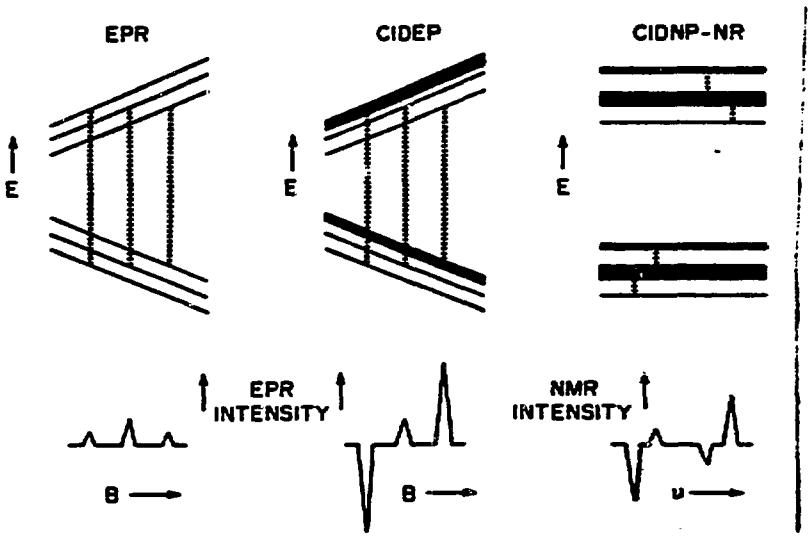

Figure 8. Comparison of spin population as observed in EPR experiments on $\cdot CH_2OH$ radical with Boltzmann population (left), with CIDEP (middle), and as observed by NMR-NR (right).

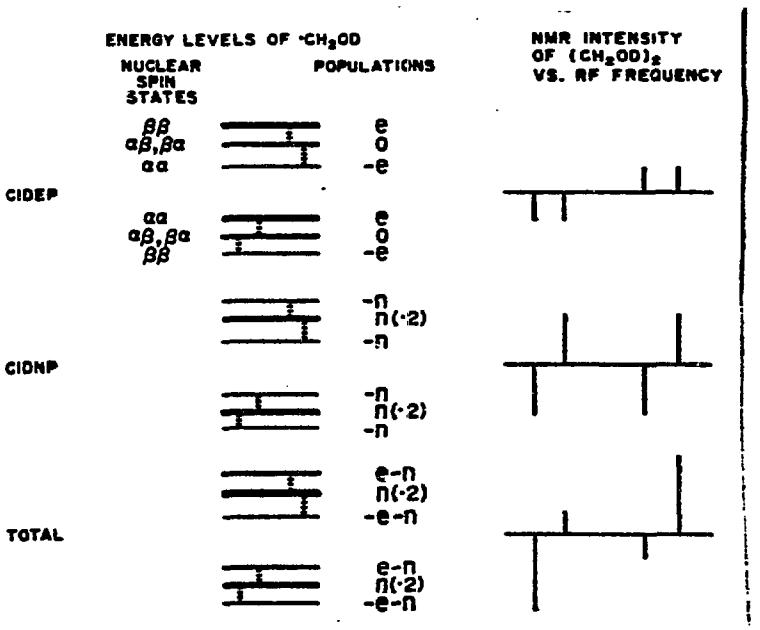

Figure 9. Population schemes as observed in NMR-NR showing how CIDEP and CIDNP contributions are combined.

fields, the CIDEP spectrum of $\cdot CH_2OD$ at ca. 10 GHz consists of a triplet with the low field line in emission and the high field line in enhanced absorption. Figures 8 and 9 depict a population scheme consistent with this observed CIDEP, and a scheme with the additional features necessary to also be consistent with the NMR-NR spectrum.

It is also of interest to identify the radical pair interactions responsible for NMR-NR. The possible sources of polarization in $\cdot CH_2OD$ radicals which could yield ethylene glycol are specified in Eqs. 16-18. Interactions with $\cdot OH$ are not expected to contribute to polarization due to rapid relaxation in $\cdot OH$ (9). The CIDNP polarizations indicated (A = enhanced absorption, 0 = none) are those based on simple rules (8) for predicting high field CIDNP. No CIDNP multiplet effect is observable by NMR in ethylene glycol since the NMR spectrum consists of a single line.

$$\overline{e^-_{aq} + \cdot CH_2OD} \xrightarrow{\text{escape}} \cdot CH_2OD \xrightarrow{\cdot CH_2OD} (CH_2OD)_2 \ (A) \qquad (16)$$

$$\overline{D\cdot + \cdot CH_2OD} \xrightarrow{\text{escape}} \cdot CH_2OD \xrightarrow{\cdot CH_2OD} (CH_2OD)_2 \ (A) \qquad (17)$$

$$\overline{\cdot CH_2OD + \cdot CH_2OD} \begin{cases} \xrightarrow{\text{cage}} (CH_2OD)_2 \ (0) & (18a) \\ \xrightarrow{\text{escape}} \cdot CH_2OD \xrightarrow{\cdot CH_2OD} (CH_2OD)_2 \ (0) & (18b) \end{cases}$$

At fields above about 75 mT, ethylene glycol is found to have a CIDNP spectrum in enhanced absorption. This observation shows that the radical pair in pathway 16 must be involved. In neutral solution, the relative yields of radicals $\cdot CH_2OD$ and $\cdot D$ are approximately 2.7 and 0.6, respectively, favoring pathway 16 over pathway 17. The g-value difference Δg between the members of the radical pair is much larger in pathway 16, also favoring this route as a source of polarization. However, if the NMR-NR effect were primarily due to the $e^-_{aq} + \cdot CH_2OD$ pair, a detectable NMR-NR net CIDNP effect (n_N) would be predicted by Eq. 15. Thus, it is likely that the most effective polarization pathway giving rise to the spin populations observed by NMR-NR is via the pair $\cdot CH_2OD + \cdot CH_2OD$, for which $\Delta g = 0$. Evaluation of a_n for each spin state of the radical pair (Eq. 15) shows that even though no CIDNP multiplet effect is observable in ethylene glycol, the nuclear states of the pair still differ in their reaction rates and that the nuclear levels of $\cdot CH_2OD$ are depopulated at different rates. The

perturbing rf pulses permit NMR detection of this polarization, as well as the CIDEP polarization. The CIDNP multiplet effect predicted for the escaping radicals has the same sign of n_M as that observed (opposite to that predicted for the cage reaction). This is reasonable since the time of rf irradiation (effective pulse length) can be much longer for the longer-lived escaping radicals, allowing partial saturation to occur. This conclusion is also consistent with the time dependence of the NMR-NR effect, which appears to follow second order kinetics (with a half life of about 6 μs at the radical concentrations used).

In summary, the spin populations in a transient radical observed using NMR-NR can be explained using the radical pair theory of CIMP. The multiplet effects in both CIDEP and CIDNP have been observed for a symmetric radical pair using NMR-NR. As illustrated, the CIDNP and CIDEP contributions to the spin populations of transient radicals observed by NMR-NR are separable. Experiments are in progress to measure other types of spin systems, to extract the kinetics of the CIDEP and CIDNP processes, and to find out how the radical chemistry of the given system is revealed through the variation in the electron/nuclear population ratios. We believe that the NMR-NR technique will develop into a powerful new technique for the study of transient radicals in solution in both radiation and photochemistry.

ACKNOWLEDGMENT

Work supported by the Office of Basic Energy Sciences, Division of Chemical Sciences, U. S. Department of Energy, under Contract W-31-109-Eng-38.

REFERENCES

(1) Trifunac, A.D. and Thurnauer, M.C.: 1979, *Time Domain Electron Spin Resonance*, ed. L. Kevan and R. N. Schwartz, John Wiley & Sons, Inc., New York.
(2) Trifunac, A.D., Norris, J.R., and Lawler, R.G.: 1979, J. Chem. Phys. 71, p. 7380.
(3) Syage, J.A., Lawler, R.G., and Trifunac, A.D., to be published.
(4) Trifunac, A.D. and Evanochko, W.T.: 1980, J. Am. Chem. Soc. 102, p. 4598.
(5) (a) Breit, G. and Rabi, I.I.: 1931, Phys. Rev. 38, p. 2082. (b) Poole, C.P. and Farach, H.A.: 1972, *The Theory of Magnetic Resonance*, Wiley-Interscience, New York, p. 203.
(6) Laroff, G.P. and Fessenden, R.W.: 1973, J. Phys. Chem. 77, p. 1283.

(7) Nuttall, R.H.D. and Trifunac, A.D.: 1981, Chem. Phys. Lett. 81, 151 (1981).
(8) *Chemically Induced Magnetic Polarization*: 1977, L. T. Muus *et al.*, eds. (NATO ASI), D. Reidel, Publishers, Dordrecht.
(9) (a) Verma, N.C. and Fessenden, R.W.: 1976, J. Chem. Phys. 65, p. 2139.
(b) Trifunac, A.D., Johnson, K.W., Clifft, B.E., and Lowers, R.H.: 1975, Chem. Phys. Lett. 35, p. 566.
(10) Ivan, Y., Rabani, J., and Henglein, A.: 1976, J. Phys. Chem. 80, p. 1558.